| Title | Optimization of Link Member of Eccentrically Braced Frames for Maximum Energy Dissipation |
|---|---|
| Auther(s) | Ohsaki, M.; Nakajima, T. |
| Citation | Journal of Constructional Steel Research , 75 : 38 - 44 |
| Issue Date | 2012-08 |
| DOI | 10.1016/j.jcsr.2012.03.008 |
| Self DOI | |
| URL | http://ir.lib.hiroshima-u.ac.jp/00046722 |
| Right | Copyright (c) 2012 Elsevier Ltd. This is not the published version. Please cite only the published version. この論文は出版社版でありません。引用の際には出版社版をご確認ご利用ください。 |
| Relation | |

# Optimization of Link Member of Eccentrically Braced Frames for Maximum Energy Dissipation

M. Ohsaki[a,*], T. Nakajima[b,1]

[a]*Dept. of Architecture, Hiroshima University, Higashi-Hiroshima, Japan*
[b]*Dept. of Architecture and Architectural Engineering, Kyoto University, Kyoto, Japan*

## Abstract

An optimization method is presented for design of an eccentrically braced frame (EBF), which is used as a passive control device for seismic design of building frames. The link member between the connections of beams and braces of EBF is reinforced with stiffeners in order to improve its stiffness and plastic deformation capacity. We present a method for optimizing the locations and thicknesses of the stiffeners of the link member. The optimal solutions are found using a heuristic approach called tabu search. The objective function is the plastic dissipated energy before failure. The deformation of the link member under static cyclic loads is simulated using a finite element analysis software package. It is demonstrated in the numerical examples that the dissipated energy can be increased through optimization within small number of analyses.

*Keywords:* Eccentrically braced frame, Link member, Energy dissipation, Shape optimization, Tabu search

## 1. Introduction

Owing to recent development of computer technologies as well as the algorithms for analysis and structural optimization, we can optimize complex structures using sophisticated finite element (FE) analysis for evaluation of elastoplastic responses. For example, the body of a vehicle can be optimized

considering crash properties [1, 2]. However, most of the optimization approaches based on FE-analysis have been developed for application to problems with simple elastic responses [3].

In the conventional formulations of optimization problems in the field of building engineering, the stiffnesses of beams and columns of frames are optimized to minimize the total structural volume under constraints on elastic stresses and displacements against static loads [4]. However, one of the criticisms on optimization in building engineering is that the structures in this field should be designed considering large uncertainty in loads and materials, and the structures should be robust against all possible load types.

Substantial effort has been made over the decades for optimizing the structural parts and components such as beams, columns, and joints, in civil and architectural engineering. Recently, numerical optimization methods have been proposed using heuristic approaches and sophisticated finite element models [5]. It is worthwhile to spend much computational effort for optimization of structural parts, because they are mass-products and the design loads and deformation demands on structural parts are much simpler than those for the building structure. The authors optimized the cross-sectional shape of the clamping device of a frame-supported membrane structure [6]. The first author optimized the flange shape of a beam with reduced section for maximization of plastic energy dissipation under static monotonic loads [7] and cyclic loads [8]. However, in their study, a heuristic approach called simulated annealing is used, and more than thousand analyses are required for optimization. Therefore, it is important to develop a computationally efficient algorithm for optimizing structural parts considering complex elastoplastic responses.

Eccentrically connected braces are effectively used as a passive control device for dissipating seismic energy in the link member between the connections of beams and braces. A frame with such braces is called an eccentrically braced frame (EBF). The link member should have enough energy dissipation capacity before ductile failure to prevent collapse of the frame. Therefore, seismic performance may be improved through optimization of link member for maximizing ductility and energy dissipation. Prinz and Richards [9] studied the effect of web-opening in the link member of an EBF by carrying out parametric study on the number and locations of the openings. They concluded that opening holes in the web is not effective, because stress concentration may occur around the hole leading to premature failure of the link. Okazaki and Engelhardt [10] carried out cyclic loading tests for 37 specimens

2

of link member with various types of stiffeners, steel materials, and loading protocols. They found that the fracture in the web of link member can be delayed by appropriately modifying the locations of stiffeners.

In this study, we present a method for optimizing the link member of an EBF. The deformation of the link member under static cyclic loads is simulated using the commercial FE-analysis software package ABAQUS Ver. 6.10.3 [11]. The failure of the link member is predicted by the *failure index* defined by the triaxiality of the stress field and the accumulated plastic strain in tension and compression [12, 13]. The objective function is the dissipated energy before failure of the link member. The design variables are the locations and thicknesses of the stiffeners. An approximate optimal solution is found using a heuristic approach called tabu search. The accuracy of FE-analysis as well as failure index is verified in comparison to the experimental results in [10] under forced static cyclic deformations with increasing amplitude at the beam ends. It is demonstrated in the numerical examples that the dissipated energy before failure can be increased through optimization with small number of analyses, although global optimality of the solution is not guaranteed.

## 2. Failure analysis of eccentrically braced frames

Consider an EBF as shown in Fig. 1 with two braces that are connected eccentrically to the beams in each story. The typical dimension of the frame is indicated in comparison to the length $e$ of the link member. The link member between the connections of beams and braces is supposed to dissipate seismic input energy by plastic deformation. Stiffeners are attached in one side of a link member, which is subjected to cyclic forced deformation. The ductility of the member is defined, as follows, using the failure index.

The responses of the link under pseudo-static loading are simulated by FE-analysis using shell elements. The state variables such as stresses and strains, which are functions of pseudo-time $t$, are evaluated at each integration point. Let $\varepsilon_\mathrm{p}(t)$ denote the equivalent plastic strain defined as

$$\varepsilon_\mathrm{p}(t) = \int_0^t \sqrt{\frac{2}{3}\dot{\varepsilon}_{ij}^\mathrm{p}(\tau)\dot{\varepsilon}_{ij}^\mathrm{p}(\tau)}\mathrm{d}\tau \tag{1}$$

where $\varepsilon_{ij}^\mathrm{p}(t)$ is the plastic strain tensor, $\dot{(\ )}$ is the derivative with respect to time, and the summation convention is used. The equivalent plastic strain
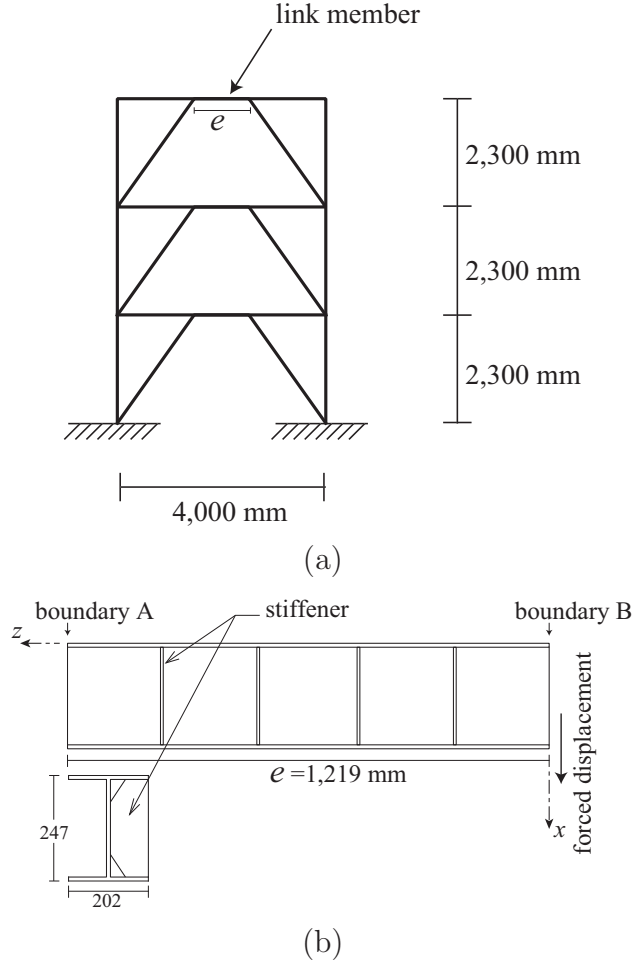
Figure 1: An eccentrically braced frame; (a) frame model, (b) link member.

represents amount of plastic deformation in material level, and is evaluated at each integration point. Many fracture criteria have been presented using $\varepsilon_\mathrm{p}(t)$. In the following, the argument $t$ is omitted for brevity.

   We use an extended version of the SMCS criterion that was developed for simulating ductile fracture of metals due to void growth [12, 13]. The critical plastic strain $\varepsilon^\mathrm{cr}$ is first defined as

$$\varepsilon^\mathrm{cr} = \alpha \exp\left(-1.5\frac{\sigma_\mathrm{m}}{\sigma_\mathrm{e}}\right) \tag{2}$$

4

where $\sigma_m$ is the mean stress, and $\sigma_e$ is the von Mises equivalent stress. The parameter $\alpha$ is dependent on material. Eq. (2) indicates that the critical plastic strain for ductile fracture depends on the stress triaxiality $\sigma_m/\sigma_e$. Then the failure index for monotonic loading is defined as

$$I_f = \frac{\varepsilon_p}{\varepsilon^{cr}} \tag{3}$$

The material is assumed to fracture when $I_f$ reaches 1.0. As seen from (2) and (3), $\varepsilon^{cr}$ has a smaller value if the material is in tensile state and $\sigma_m$ has a larger positive value.

The formulations (2)–(3) are based on the ductile fracture due to void growth under monotonic tensile deformation. Accordingly, the failure index $I_f$ does not incorporate the effect of cyclic loading, where the void shrinks due to compressive plastic loading. Therefore, we use the following formulation by Kanvinde and Deierlein [14]. The equivalent plastic strain $\varepsilon_p$ is divided into $\varepsilon_t$ ($> 0$) and $\varepsilon_c$ ($> 0$) that are accumulated during tensile and compressive plastic loading states, respectively, which are identified by the sign of $\sigma_m$. The *significant* plastic strain $\varepsilon^*$, which represents the amount of void growth, is defined as

$$\varepsilon^* = \varepsilon_t - \varepsilon_c \tag{4}$$

The critical value $\varepsilon^{cr*}$ for $\varepsilon^*$ is given as

$$\varepsilon^{cr*} = \exp\left(-\lambda\varepsilon_p\right)\varepsilon^{cr} \tag{5}$$

where $\lambda$ is a positive material parameter. As is seen from (5), $\varepsilon^{cr*}$ is smaller than $\varepsilon^{cr}$, and decreases in accordance with an increase of $\varepsilon_p$. Ductile fracture is assumed to occur when the cyclic failure index $I_f^*$, defined as follows, reaches 1.0:

$$I_f^* = \frac{\varepsilon^*}{\varepsilon^{cr*}} \tag{6}$$

The rotation angle $\gamma$ of link is defined, as follows, using the length $e$ and the relative transverse displacement $\delta$, calculated as the difference between the vertical displacements at the two ends:

$$\gamma = \frac{\delta}{e} \tag{7}$$

Let $V$ and $k_e$ denote the shear force and initial value of the stiffness $V/\gamma$ of the link. The plastic component $\gamma_p$ of rotation angle is calculated by
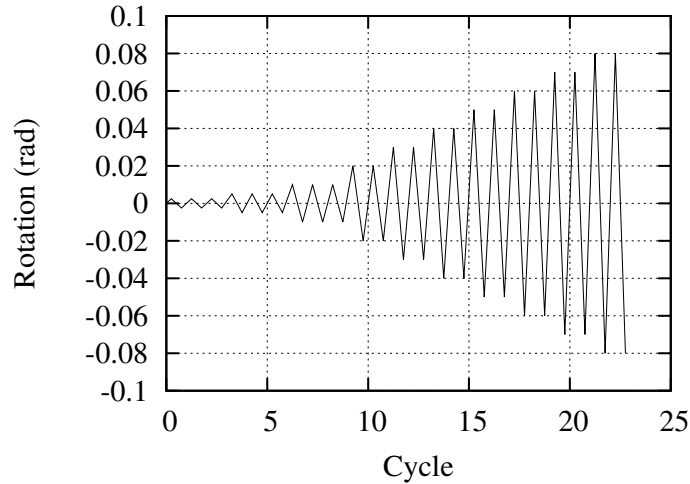
Figure 2: Loading protocol for experiment [10].

subtracting the elastic component $V/k_\mathrm{e}$ from the total value $\gamma$ as

$$\gamma_\mathrm{p} = \gamma - \frac{V}{k_\mathrm{e}} \tag{8}$$

According to American Institute of Steel Construction (AISC) [15], the strength and failure mode of a link member depend on the length $e$ as well as the ratio of the fully plastic moment $M_\mathrm{p}$ to the shear strength $V_\mathrm{p}$. In this paper, we consider a short link with moderately large $M_\mathrm{p}/V_\mathrm{p}$, which is classified to exhibit shear/bending failure mode. The loading capacity of a short link is restricted by the elastoplastic buckling of the web and flange. The demand for rotation angle of this link varies between 0.02 and 0.08 as a linear function of $M_\mathrm{p}/V_\mathrm{p}$. Okazaki $et\ al.$ [10] conducted a series of cyclic tests for link under four types of loading protocol. We use the results of monotonically increasing amplitude, as shown in Fig. 2, for verification of the material model and identification of the parameters in failure index.

The general purpose FE-analysis software package ABAQUS Ver. 6.10.3 [11] is used for static elastoplastic analysis. The shell elements S4R and S3R with linear interpolation and reduced integration are used, as shown in Fig. 3, for modeling the link member, because triangular and quadrilateral elements are automatically selected through mesh generation by Python script.
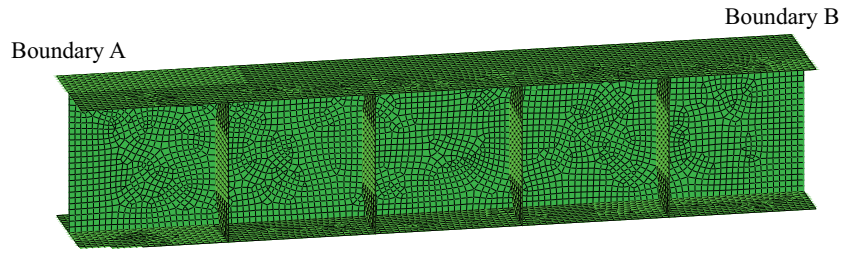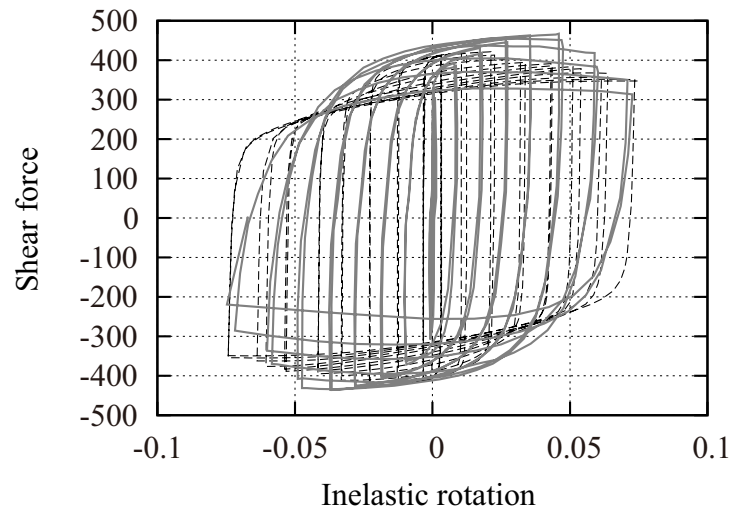
6

Figure 3: FE-mesh of link member.



Figure 4: Comparison of force-rotation relation to experimental result in [10]; thick gray line: experiment, dotted line: analysis ($S = 0.01$ m).

The link member has the wide-flange section W10×33, which is denoted as H-247×202×7×11 in Japanese specification. However, the measured dimensions are used for the section of beam; i.e., the thicknesses of web and flange are 8.1026 mm and 11.306 mm, respectively [16]. The link member has four equally spaced stiffeners of thickness 10.0 mm on one side, and length $e$ =1219 mm.

The material is ASTM A992, where Young's modulus is $2.0 \times 10^5$ N/mm$^2$ and Poisson's ratio is 0.3. The values of yield stress $\sigma^{\mathrm{y}}$ and tensile strength $\sigma^{\mathrm{u}}$ (N/m$^2$) obtained by uniaxial tests for web and flange are $(\sigma^{\mathrm{y}}, \sigma^{\mathrm{u}}) = (4.02 \times 10^8, 5.30 \times 10^8)$ and $(3.79 \times 10^8, 5.18 \times 10^8)$, respectively. The same material as
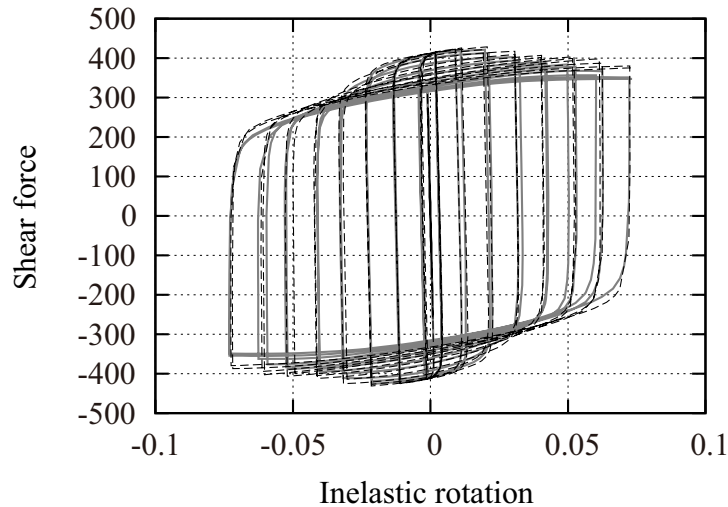
7

Figure 5: Comparison of analysis results of force-rotation relation with different mesh sizes; thick gray line: $S = 0.01$ m, dotted line: $S = 0.02$ m.

web is used for the stiffener. The bilinear relation with kinematic hardening with coefficient 0.006 is used assuming that the maximum stress is attained at the plastic strain equal to 0.15. The parameter $\alpha$ for the failure index is 2.6 as identified in Ref. [13].

All the translational and rotational displacement components are fixed at boundary 'A' in Fig. 3 except the displacement in $z$-direction (axial direction). A forced cyclic displacement in $x$-direction (vertical direction) is given at boundary 'B'.

After defining the geometry of the beam, finite-element mesh is automatically generated, where the accuracy of analysis can be controlled by the nominal size $S$ in the process of mesh generation; i.e., the mesh is generated so that the average size of an element is equal to $S$. In the following examples, $S = 0.01$ m is given to have about 25 elements in the vertical direction of the web, and 20 elements in the transverse direction of the flange. The relation between shear force and inelastic rotation of Type-6B in Ref. [10] is plotted in thick gray line in Fig. 4, while the dotted line shows the analysis result, which has moderately good agreement with the experimental result, although the numerical result has larger strength in the first few cycles, and smaller strength in the subsequent cycles. Fig. 5 compares the numerical
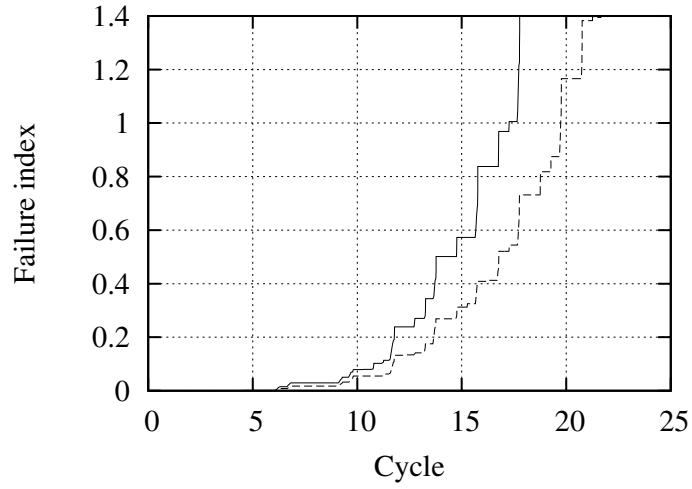
8

Figure 6: Histories of maximum failure index by FE-analysis of the experimental model; solid line: $S = 0.01$ m, dotted line: $S = 0.02$ m.
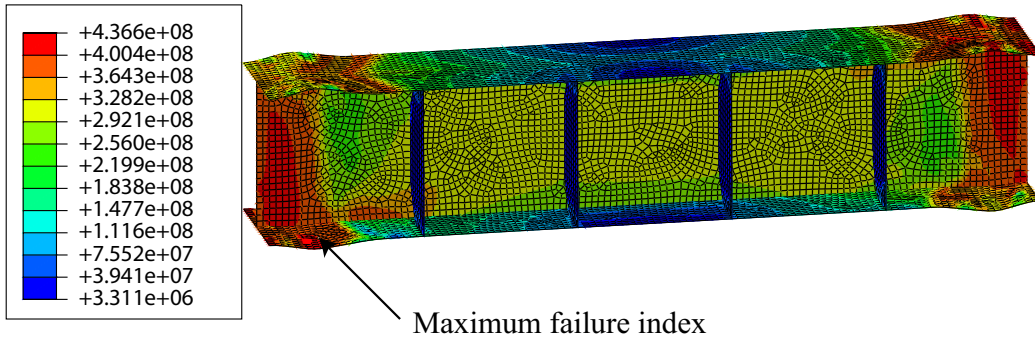


Maximum failure index

Figure 7: Stress distribution of experimental model at cycle 16.944.

results with $S = 0.01$ m (thick gray line) and $0.02$ m (dotted line), which do not have much difference.

According to Kanvinde and Deierlein [14], the parameter $\lambda$ for the failure index may vary between 2.5 and 8.0. In the following, an intermediate value 4.0 is used for $\lambda$. Fig. 6 shows the histories of maximum values of failure index $I_{\mathrm{f}}^*$ among all elements for $S = 0.01$ m and $0.02$ m. As is seen, the maximum failure index becomes larger as the mesh size becomes smaller.
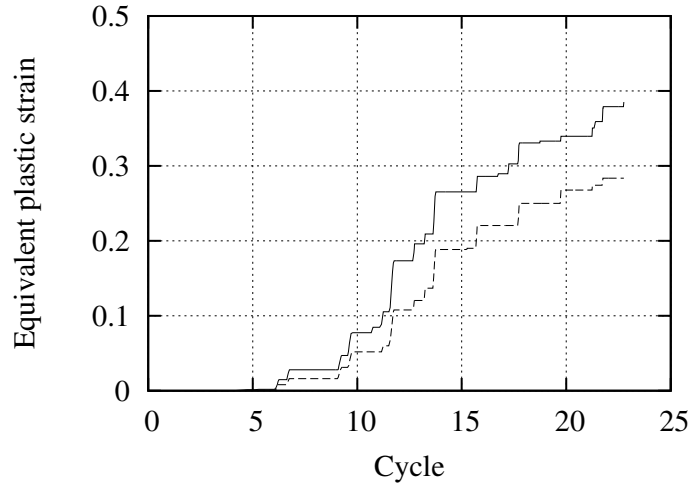
9

Figure 8: Histories of maximum equivalent plastic strain by FE-analysis of the experimental model; solid line: $S = 0.01$ m, dotted line: $S = 0.02$ m.
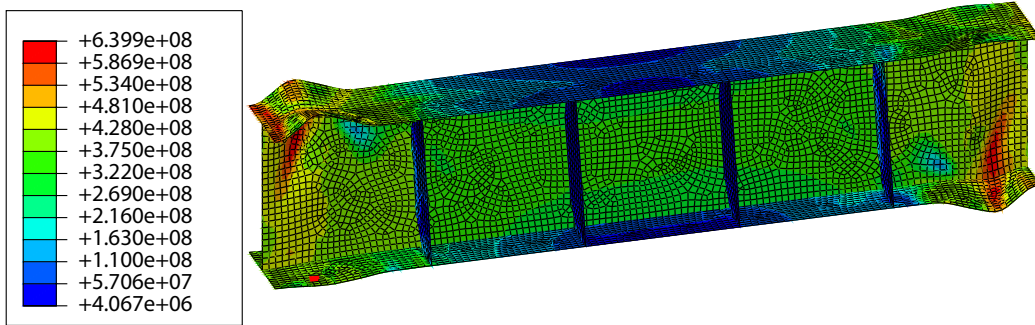


Figure 9: Stress distribution of experimental model at the final state (cycle 22.25).

For $S = 0.01$ m, the failure index reaches 1.0 at cycle 16.944 at the element indicated in Fig. 7, which is located in the flange that exhibits local buckling. In contrast, for $S = 0.02$ m, the failure index reaches 1.0 at cycle 20.756 at the element located in the web at the beam end. Therefore, the location of failure has been successfully found with $S = 0.01$ m; hence, we use $S = 0.01$ m in the following examples. Fig. 8 shows the histories of maximum values of equivalent plastic strain, which shows that the results with $S = 0.01$ m have larger plastic strain than those with $S = 0.02$ m.

10

The deformation at the final state (cycle 22.25) is shown in Fig. 9, which exhibits local flange buckling. In this model, the number of elements is 8856, number of nodes is 9014, and number of degrees of freedom is 54084. A PC with Intel Xeon 3.33GHz and 12GB memory is used for computation. Although the PC has six cores, only single core is available for computation using ABAQUS, and the CPU time is 7764.2 s.

## 3. Formulation of optimization problem and optimization method

### 3.1. Optimization problem

We optimize the locations and thicknesses of stiffeners of the link beam for maximization of plastic dissipated energy before the failure index reaches 1.0. Since the optimization problem is highly nonlinear, and demands much computational cost for evaluation of the objective function, we use a heuristic approach called tabu search (TS), which can obtain an approximate optimal solution within small number of analyses. TS has successfully been applied to optimization problems with integer variables [17]. Therefore, the variables are discretized into integer values.

Let $\mathbf{J} = (J_1, \ldots, J_m)$ denote the vector of $m$ design variables. Real values $X_1, \ldots, X_m$ are defined by integer values $J_1, \ldots, J_m$ with the specified lower-bound value $X_i^0$ and increment $\Delta X_i$ as

$$X_i = X_i^0 + (J_i - 1)\Delta X_i, \quad (i = 1, \ldots, m) \tag{9}$$

Therefore, all properties of the link member are functions of $\mathbf{J}$.

We maximize the plastic energy $E_p(\mathbf{J})$ dissipated before $I_f^*(\mathbf{J})$ reaches 1.0 during the specified cyclic deformation. Let $s_i$ denote the number of sampling values that $J_i$ can take. The optimization problem is formulated as follows as an unconstrained problem:

$$\text{Maximize} \ \ F(\mathbf{J}) = E_p(\mathbf{J}) \tag{10a}$$

$$\text{subject to} \ J_i \in \{1, \ldots, s_i\}, \ (i = 1, 2, ..., m) \tag{10b}$$

### 3.2. Optimization method

TS is classified as a single-point search heuristic approach, which is a slight extension of the random local search [4, 17]. In contrast to a population-based approach such as genetic algorithm, TS has single solution at each step of local search. Therefore, TS is more suitable than a genetic algorithm for
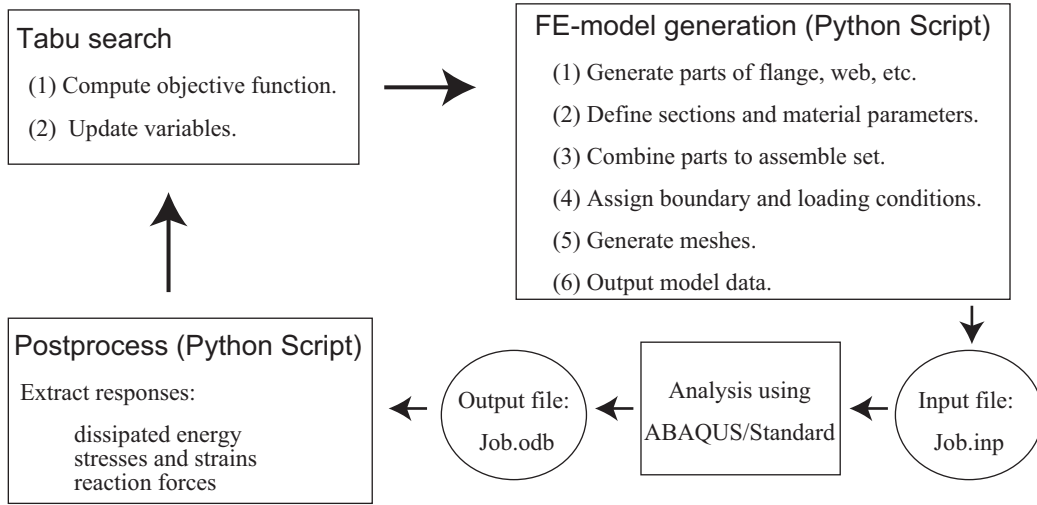
Figure 10: Optimization algorithm using TS and ABAQUS.

structural optimization problems that demand large computational cost for response evaluation. TS basically moves to the best neighborhood solution even if it does not improve the current solution. A tabu list is used to prevent an unfavorable phenomenon called cycling, in which small number of solutions are selected alternatively. The basic algorithm of TS is summarized as follows:

**Step 1** Randomly generate a seed solution $\hat{\mathbf{J}}$, and initialize the tabu list $T$ as $T = \{\hat{\mathbf{J}}\}$. Evaluate the objective function and initialize the incumbent optimal objective value as $F^{\text{opt}} = F(\hat{\mathbf{J}})$.

**Step 2** Generate a set of $q$ neighborhood solutions $N = \{\mathbf{J}_1^{\text{N}}, \ldots, \mathbf{J}_q^{\text{N}}\}$ from $\hat{\mathbf{J}}$, and evaluate the objective value of each solution.

**Step 3** Among the solutions in the set $N$, select the best one that has the maximum value of $F(\mathbf{J}_j^{\text{N}})$, and is not included in the list $T$. Assign the best solution as the new seed solution $\hat{\mathbf{J}}$.

**Step 4** Update the incumbent optimal objective value as $F^{\text{opt}} = F(\hat{\mathbf{J}})$, if $F(\hat{\mathbf{J}}) > F^{\text{opt}}$.

**Step 5** Add $\hat{\mathbf{J}}$ to the list $T$. Remove the oldest solution from $T$, if the number of solutions in $T$ exceeds the specified limit.

12

**Step 6** Output $F^{\text{opt}}$ and the corresponding optimal solution, if the number of iterations reaches the specified value; otherwise, go to Step 2.

The definition of neighborhood is problem dependent. For variables with simple integer values, the neighborhood values of $J_i$ at the current value $k$ may be given as $J_i = k - 1$, $k$, $k + 1$. Therefore, we have at most $3^m$ neighborhood solutions for a problem with $m$ variables. It is desirable to search all the neighborhood solutions when selecting the next seed solution. However, one of the purpose of this study is to show that the complex performance of a structure can be improved through small number of analyses; therefore, we limit the neighborhood solutions to a very small size.

Fig. 10 shows the data flow between TS and FE-analysis using ABAQUS. The pre-process and post-process are carried out using the Python script. The computations of functions and the process of TS are coded using Fortran.

## 4. Optimization of link member

The link member to be optimized has the same wide-flange section W10×33 as the experimental model. Thicknesses of web and flange are their nominal values 7.366 mm and 11.050 mm, respectively. The standard solution of the link member has four equally spaced stiffeners of thickness 10.0 mm in one side, and the length $e = 1219$ mm. Accordingly, the link member has the ratio $M_{\text{p}}/V_{\text{p}} = 639$ mm, which is classified to exhibit shear/bending failure mode.

The material is ASTM A992, which is the same as the experimental model. Young's modulus is $2.0 \times 10^5$ N/mm$^2$ and Poisson's ratio is 0.3. The nominal value 359.0 N/mm$^2$ is taken for the yield stress for web, flange, and stiffener, and the hardening coefficient is 0.006. The same parameter values $\alpha = 2.6$ and $\lambda = 0.4$ as the experimental model are used for the failure index.

The locations and thicknesses of the four stiffeners are optimized. In order to preserve the symmetry, the independent variables for the locations $X_i$ (mm) are defined by the two integer variables $J_1$ and $J_2$ as

$$X_i = X_i^0 + (J_i - 6)\Delta X_i, \quad J_i \in \{1, \ldots, 11\}, \quad (i = 1, 2) \tag{11}$$

where $X_i^0$ is the location of the standard model, and $\Delta X_1 = \Delta X_2 = 20$ (mm). Therefore, the lower and upper bounds for $(X_i - X_i^0)$ are $-100$ mm and 100 mm, respectively.
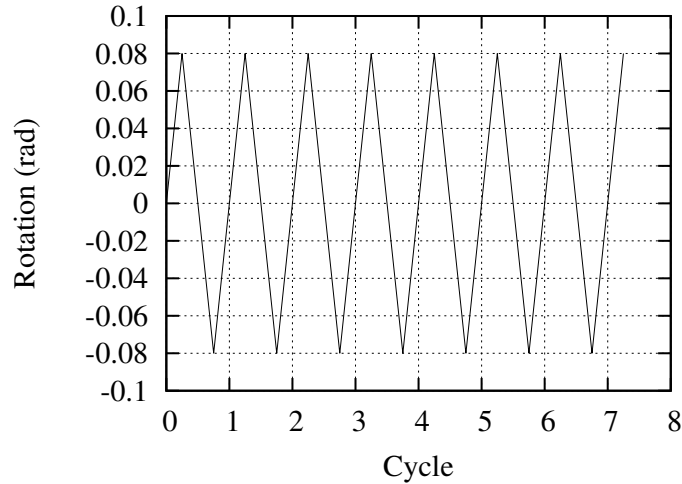
Figure 11: Forced cyclic rotation angle of the beam.

The thicknesses $X_i$ (mm) of the stiffeners are defined by the variables $J_3$ and $J_4$ as

$$X_i = X_i^0 + (J_i - 3)\Delta X_i, \quad J_i \in \{1, \ldots, 7\}, \quad (i = 3, 4) \tag{12}$$

where $X_i^0$ is 10 mm, and $\Delta X_3 = \Delta X_4 = 3$ (mm); hence, the lower and upper bounds of $X_i$ are $-4$ mm and 22 mm, respectively.

The loading protocol is shown in Fig. 11, which has a constant amplitude $\pm 0.08$ of the rotation angle. For the TS, the number of neighborhood solutions is 5, number of steps is 10, and the size of tabu list is 50. Although the solution obtained by TS is not the global optimum, the best solution during all steps is hereafter called optimal solution. Fig. 12 shows the stresses of the standard solution at cycle 4.2565, when $I_f^*$ reaches 1.0 at a web element connected to the flange, as indicated in Fig. 12. As is seen, local buckling occurs at the flange near the beam end.

Optimal solution has been found from the standard solution as the initial solution. Five solutions were rejected by the tabu list. The optimal locations of four stiffeners are $(-80, -40, +40, +80)$ (mm), relative to the standard solution, and the optimal thicknesses are (22,10,10,22) (mm), while the thicknesses of the standard solution are (10,10,10,10) (mm). Fig. 13 shows the stresses of the optimal solution at cycle 6.2690, when $I_f$ reaches
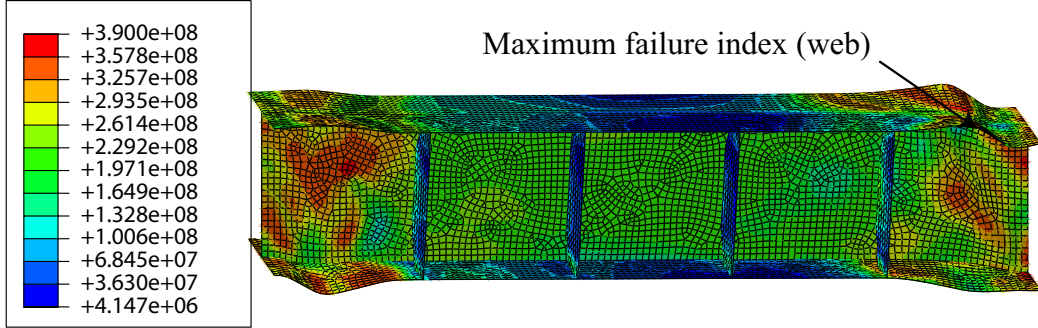
14

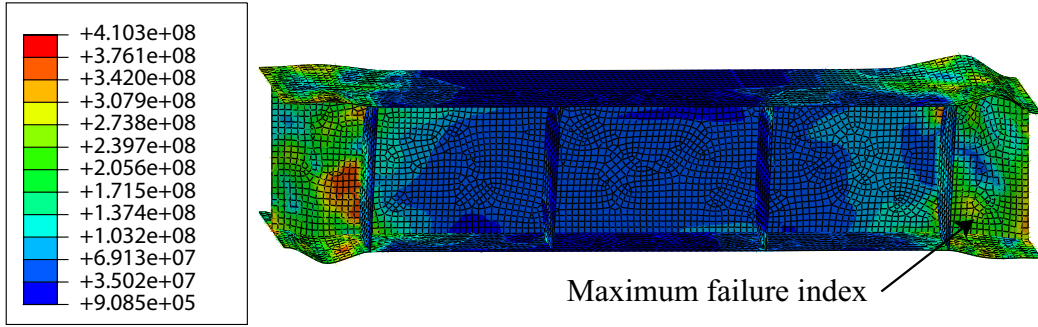Figure 12: Stress distribution of standard solution when $I_\mathrm{f}^*$ reaches 1.0.



Figure 13: Stress distribution of optimal solution when $I_\mathrm{f}^*$ reaches 1.0.

Table 1: Optimization results

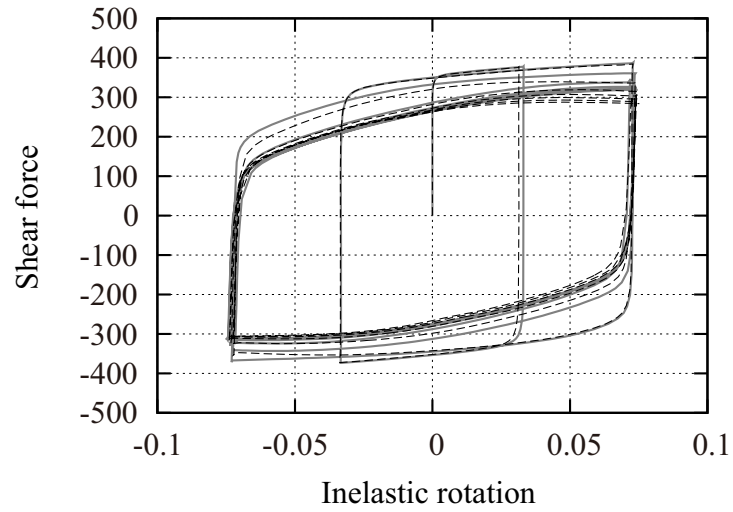| model | cycle | $R_{\max}$ (kN) | $E_\mathrm{p}$ (kN· m) | $E_\mathrm{p}^{\text{final}}$ (kN· m) | $I_\mathrm{f}^{*\text{final}}$ |
|---|---|---|---|---|---|
| Standard | 4.2565 | 384.27 | 401.65 | 678.73 | 3.7577 |
| Optimal | 6.2690 | 388.93 | 601.49 | 696.40 | 2.4182 |
| Intermediate | 5.2615 | 385.71 | 486.78 | 670.56 | 2.1564 |
| Standard (incremental) | 16.755 | 363.72 | 368.79 | 841.81 | 16.543 |
| Optimal (incremental) | 21.242 | 365.40 | 760.38 | 908.25 | 2.91226 |

15

Figure 14: Comparison of analysis results of force-rotation; thick gray line: optimal solution, dotted line: standard solution.
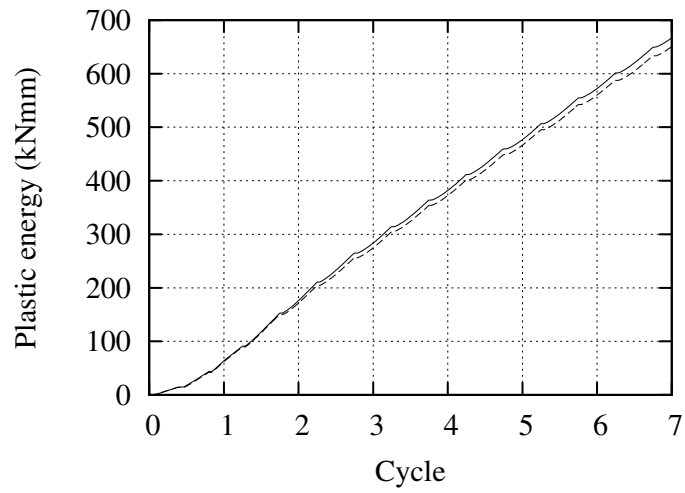


Figure 15: Histories of plastic dissipated energy; solid line: optimal solution, dotted line: standard solution.
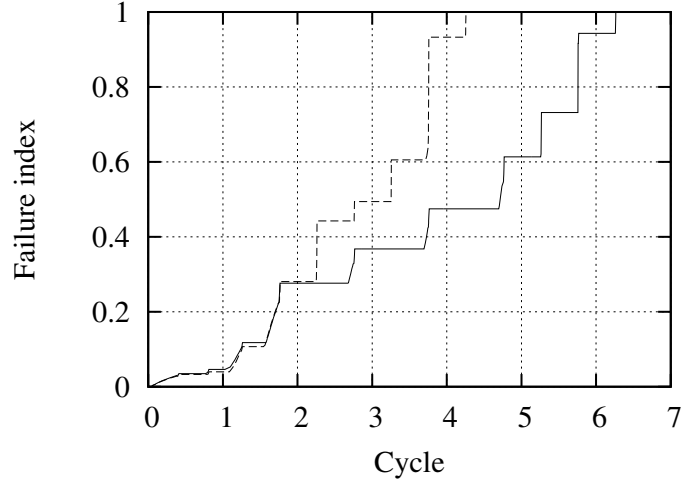
16

Figure 16: Histories of maximum failure index; solid line: optimal solution, dotted line: standard solution.

1.0 at an element in the web near the beam end. Although the failure of the optimal solution is determined by local buckling near the beam ends, which is similar to the standard solution, the optimal solution has two more cycles than the standard solution before the failure index reaches 1.0. We can see from these results that the two stiffeners become thicker and move to the ends, where the standard solution have large deformation. The responses of the solutions are listed in Table 1, dissipated energy before $I_f^*$ reaches 1.0 increased about 50% from the standard solution; hence, the energy dissipation property can be drastically improved through optimization. It is also seen from Table 1 that the maximum value $R_{\max}$ of the reaction force becomes slightly larger as the result of optimization. Fig. 15 shows the histories of plastic energy dissipation of the optimal and initial solutions, which confirms that energy dissipation property is slightly improved through optimization. Therefore, the energy dissipation property has been improved mainly due to enhancement of ductility rather than strength. Fig. 16 shows the history of failure index with respect to cycle number. As is seen, increase of failure index is successfully suppressed through optimization.

The dissipated energy $E_p^{\text{final}}$ and the failure index $I_f^{*\text{final}}$ at the final state (cycle 7.25) is also listed in Table 1. Since the fracture of material is not incorporated in the constitutive model of steel, the dissipated energy un-

til the final state of the initial and optimal solutions are almost the same; however, the failure index at the final state has been reduced through optimization. The moment-rotation relations are compared in Fig. 14 for initial and optimal solutions. As is seen, the peak moment has not been improved through optimization, but the deterioration after cyclic deformation has been improved.

The intermediate solution has the mean values between the standard and optimal solutions; i.e., the locations of four stiffeners are $(-40, -20, +20, +40)$ (mm), and the thicknesses are $(16, 10, 10, 16)$ (mm). As expected, all responses except the final failure index of the intermediate solution have the values between those of standard and optimal solutions, which verifies the reliability of the FE-analysis.

## 5. Conclusions

It has been shown in this paper that the plastic energy dissipation property of a link member of an EBF can be drastically improved by optimizing the locations and thicknesses of the stiffeners. The link member is subjected to cyclic forced deformation, and its failure is defined using the failure index. The elastoplastic responses are evaluated using a commercial software package called ABAQUS. The accuracy of the material model is verified and the parameters for failure index are identified using the existing experimental results.

It has been demonstrated that TS is very effective for structural optimization problem, for which substantial computational cost is needed for function evaluation. Although the global optimality is not guaranteed, it is important that the performance of the structure is drastically improved within small number of analyses. The software package ABAQUS and the algorithm of TS are combined using the Python script available in ABAQUS.

Although this paper showed only one example of optimization of a structural part, it is very important to demonstrate that a passive control device can be optimized using an FE-analysis software package within a practically acceptable computational cost. This way, some of physical experiments for developing such devices can be replaced by numerical experiments, and the cost and time period for the development of a new device may be drastically reduced.

**REFERENCES**

[1] M. Avalle, G. Chiandussi, G. Belingardi, Design optimization by response surface methodology: Application to crashworthiness design of vehicle structures, Struct. Multidisc. Optim. 24 (2002) 325–332.

[2] C. H. Kim, A. R. Mijar, J. S. Arora, Development of simplified models for design and optimization of automotive structures for crashworthiness, Struct. Multidisc. Optim. 22 (2001) 307–321.

[3] M. P. Bendsøe, O. Sigmund, Topology Optimization: Theory, Methods and Applications, Springer, Berlin, 2003.

[4] M. Ohsaki, Optimization of Finite Dimensional Structures, CRC Press, 2010.

[5] N. D. Lagaros, L. D. Psarras, M. Paradrakakis, G. Panagiotou, Optimum design of steel structures with web opening, Eng. Struct. 30 (2008) 2528–2537.

[6] J. Fujiwara, T. Nakajima, M. Ohsaki, F. Takeda, Shape optimization of clamping members of frame-supported membrane structures under stress constraints, in: Proc. 6th China-Japan-Korea Joint Symposium on Optimization of Structural and Mechanical Systems (CJK-OSM6), Kyoto, Japan, 2010.

[7] P. Pan, M. Ohsaki, H. Tagawa, Shape optimization of H-beam flange for maximum plastic energy dissipation, J. Struct. Eng. 133 (8) (2007) 1176–1179.

[8] M. Ohsaki, H. Tagawa, P. Pan, Shape optimization of reduced beam section for maximum plastic energy dissipation under cyclic loads, J. Const. Steel Res. 65 (2009) 1511–1519.

19

[9] G. S. Prinz, P. W. Richards, Eccentrically braced frame links with reduced web sections, J. Constr. Steel Res. 65 (2009) 1971–1978.

[10] T. Okazaki, M. D. Engelhardt, Cyclic loading behavior of EBF links constructed of ASTM A992 steel, J. Constr. Steel Res. 63 (2007) 751–765.

[11] ABAQUS Ver. 6.10.3 Documentation, ABAQUS Inc., 2011.

[12] J. W. Hancock, A. C. Mackenzie, On the mechanism of ductile failure in high-strength steels subjected to multi-axial stress-states, J. Mech. Phys. Solids 24 (1976) 147–169.

[13] W. M. Chi, A. M. Kanvinde, G. G. Deierlein, Prediction of ductile fracture in steel connections using SMCS criterion, J. Struct. Eng. 132 (2) (2006) 171–181.

[14] A. M. Kanvinde, G. Deierlein, Micromechanical simulation of earthquake induced fracture in steel structures, Tech. Rep. TR145, Blume Center, Stanford Univ. (2004).

[15] Seismic Provisions for Structural Steel Buildings, American Institute of Steel Construction (AISC), Chicago, 2005.

[16] G. Arce, Impact of higher strength steels on local buckling and overstrength in EBFs, Master's thesis, Department of Civil Engineering, University of Texas at Austin, Austin, TX (2002).

[17] F. Glover, Tabu search: Part I., ORSA J. Computing 1 (3) (1989) 190–206.